JOURNAL OF THERMOPHYSICS AND HEAT TRANSFER
Vol. 18, No. 1, January–March 2004

Numerical Simulation of Nonequilibrium Stagnation-Line CO_2 Flows with Catalyzed Surface Reactions

P. Rini*
Université Libre de Bruxelles, 1050 Brussels, Belgium
A. Garcia† and T. Magin‡
von Kármán Institute for Fluid Dynamics, 1640 Rhode-St.-Genèse, Belgium
and
G. Degrez§
Université Libre de Bruxelles, 1050 Brussels, Belgium

A methodology developed at the Institute for Problems in Mechanics of Moscow is used for the analysis of the catalytic properties of thermal protection materials in a CO_2 environment. The method relies on a combination of 1) heat-transfer and pitot-pressure measurements in a subsonic plasma jet and 2) numerical flow simulations. The simulated environments are typical of Mars entry conditions. In particular, this work is focused on the finite-rate chemistry part of the flow description. The extension of numerical tools developed at the von Kármán Institute, required within the methodology for the determination of catalycity properties for thermal protection system materials, has been completed for CO_2 flows. Nonequilibrium stagnation-line computations have been performed for several outer edge conditions in order to analyze the influence of the chemical models for bulk reactions. Moreover, wall surface reactions have been examined, and the importance of several recombination processes has been discussed. This analysis has revealed the limits of the model currently used, leading to the proposal of an alternative approach for the description of the flow-surface interaction.

Nomenclature

C_p = mixture specific heat at constant pressure
c_i = concentration of species i
F = stream function
g = mixture nondimensional enthalpy
h = mixture enthalpy
h_i = enthalpy of species i
$\boldsymbol{J}_i$ = diffusion flux of species i
$\tilde{\mathcal{J}}_i$ = nondimensional diffusion flux of species i
K_c = equilibrium constant
k_b = backward reaction rate
k_f = forward reaction rate
M = catalyzer
M_i = molar mass of species i
$\mathcal{M}_i^{\downarrow}$ = flux of particles of species i impinging on the wall
N_r = number of reactions
N_{sp} = number of species
$\boldsymbol{n}$ = unit vector normal to the wall
n_i = number density of species i
Pr = Prandtl number
r = local radius of the probe
T = mixture temperature
u = component of the velocity in the x direction
$\tilde{V}$ = nondimensional velocity in the $\hat{\eta}$ direction
$\dot{\mathcal{W}}_i$ = nondimensional mass production term of species i
X_i = any chemical species
x = physical coordinate along the body contour
x_{ni} = element fraction of element i
y = physical coordinate normal to the body
y_i = mass fraction of species i
γ_i = recombination probability of species i
γ_i^r = recombination probability of species i involved in the rth reaction
γ_w = effective recombination probability
γ^r = rth reaction probability
$\hat{\eta}$ = second Lees–Dorodnitsyn coordinate
λ_{ij} = number of elements of type j in the species i
μ = dynamic viscosity
ν'_{ir} = stoichiometric coefficient of species i thought as reactant in reaction r
ν''_{ir} = stoichiometric coefficient of species i thought as product in reaction r
$\xi(x)$ = first Lees–Dorodnitsyn coordinate
ξ_j = number of moles of element j per unit volume
ρ = mixture density
ρ_i = partial density of species i
χ_k = rate of the kth surface reaction per unit time
$\dot{\omega}_i$ = mass production caused by chemical reactions

Subscripts

w = wall
δ = boundary-layer edge

Received 5 May 2003; presented as Paper 2003-4038 at the AIAA 34th Plasmadynamics and Lasers Conference, Orlando, FL, 23 June 2003; revision received 19 July 2003; accepted for publication 19 July 2003.

*Assistant, Service de Mécanique des Fluides, 50, Avenue F. D. Roosevelt; also Ph.D. Candidate, von Kármán Institute for Fluid Dynamics, Department of Aeronautics and Aerospace, 72, Ch. de Waterloo, 1640 Rhode-St.-Genèse, Belgium; rini@vki.ac.be. Student Member AIAA.

†Research Engineer, Department of Aeronautics and Aerospace, 72, Ch. de Waterloo; garcia@vki.ac.be.

‡Ph.D. Candidate, Department of Aeronautics and Aerospace, 72, Ch. de Waterloo; also Ph.D. Candidate, Université Libre de Bruxelles, Service de Mécanique des Fluides, 50, Avenue F. D. Roosevelt, Brussels, Belgium; magin@vki.ac.be. Student Member AIAA.

§Professor, Service de Mécanique des Fluides, 50 Avenue F. D. Roosevelt; also Adjunct Professor, von Kármán Institute for Fluid Dynamics, Department of Aeronautics and Aerospace, 72, Ch. de Waterloo, 1640 Rhode-St.-Genèse, Belgium; degrez@vki.ac.be. Associate Fellow AIAA.

Introduction

THE von Kármán Institute (VKI) has been involved since 1997 in the determination of catalytic properties of thermal-protection-system materials.

A hybrid methodology, which relies on the combination of experimental measurements and numerical calculations, has been employed for this purpose. The principles of this methodology lay on the local heat-transfer simulation (LHTS) concept developed at the Institute for Problems in Mechanics of Moscow (IPM).[1]

Recently, with the initiation of several Mars exploration projects, interest has been attracted to Mars entry problems. The two inductively coupled plasma (ICP) facilities of the Institute (Plasmatron and Minitorch) have been equipped to work with CO_2 mixtures. The VKI high-enthalpy flow solvers are interfaced with libraries to compute thermodynamic, transport, and nonequilibrium chemistry properties.[2] The thermodynamic and transport libraries have been recently updated to incorporate CO_2 mixtures.[3] In this paper the physico-chemical description of a CO_2 flow is completed, allowing for simulations in chemical nonequilibrium, characterized by both bulk and surface reactions. A critical output of the LHTS methodology is the heat load on the stagnation point of a flying body, where large gradients of temperature and mass concentrations are present. These features make this point a suitable benchmark for testing thermochemical models. The flowfield in the vicinity of the stagnation point has been analyzed by means of stagnation-line flow calculations. These computations are applied for the determination of surface catalytic efficiency in CO_2 mixtures, leading to the determination of so-called heat-flux maps.

Stagnation-Line Equations

In this section the governing equations of a mixture of reacting gases for the stagnation line flow are recalled.[4] The flow is considered steady, axisymmetric, and laminar; the influence of body forces as a result of external fields is neglected. Finally, the flow is supposed to be in chemical nonequilibrium but in thermal equilibrium.

In a classical ICP facility the material to be tested is held by a probe immersed in a low subsonic axisymmetric high-temperature jet. The heat flux is measured in the probe stagnation region. To determine the catalytic activity, it is necessary to solve the governing equations in the layer surrounding the stagnation region of the probe. If one focuses the interest only on the stagnation line, the boundary layer and the Navier–Stokes equations become equivalent, and moreover there exists a self-similar solution of the latter along the stagnation line.

Because of the combined effects of low Mach number, high temperature, high viscosity, and relatively small probe diameter, the flow Reynolds number is of the order of 100. In the classical boundary-layer theory ($R_e \gg 1$) the pressure gradient in the momentum and energy equations is computed by extrapolating the external inviscid solution to the wall.

In our case the self-similar stagnation-line flow is matched with a local-thermal-equilibrium (LTE) Navier–Stokes solution at some distance δ representative of the diffusion boundary-layer thickness. Now, the pressure gradient at this location is

$$\frac{\partial p}{\partial x} = -\rho_\delta \left(u_\delta \frac{\partial u_\delta}{\partial x} + v_\delta \frac{\partial u_\delta}{\partial y} \right) \tag{1}$$

In classical boundary-layer theory the second term is zero because $v_\delta \approx 0$. For the present low-Reynolds-number flows it is nonzero and obtained from the LTE Navier–Stokes solution.[5]

Starting from a Cartesian reference system having the x axis lying on the body surface and the y axis normal to it, the Lees–Dorodnitsyn transformation is applied to the axisymmetric boundary-layer equations, defining

$$\xi(x) = \int_0^x \rho_\delta \mu_\delta u_\delta r^2 \, \mathrm{d}s \qquad \text{and} \qquad \hat{\eta} = \mathcal{K} \frac{u_\delta r}{\sqrt{2\xi}} \int_0^y \rho \, \mathrm{d}t$$

where

$$\mathcal{K} = \frac{1}{\delta} \frac{\sqrt{2\xi}}{u_\delta r} \int_0^{\hat{\eta}_{\max}} \frac{1}{\rho} \, \mathrm{d}\hat{\eta}$$

Three new dependent variables are introduced as

$$F = \frac{u}{u_\delta}, \qquad g = \frac{h}{h_\delta}, \quad \text{and} \quad \tilde{V} = \mathcal{K} \frac{2\xi}{(\partial \xi / \partial x)} \left(F \frac{\partial \eta}{\partial x} + \frac{\rho v r}{\sqrt{2\xi}} \right)$$

Therefore, the stagnation-line equations read as follows:

Continuity:

$$\frac{\partial \tilde{V}}{\partial \hat{\eta}} + F = 0 \tag{2}$$

Species continuity:

$$\tilde{V} \frac{\partial y_i}{\partial \hat{\eta}} + \mathcal{K} \frac{\partial \tilde{\mathcal{J}}_i^{\hat{\eta}}}{\partial \hat{\eta}} = \dot{\mathcal{W}}_i \tag{3}$$

Momentum:

$$\tilde{V} \frac{\partial F}{\partial \hat{\eta}} = \frac{1}{2} \frac{\rho_\delta}{\rho} \left[1 + \frac{v_\delta}{(\partial u_\delta / \partial x)^2} \frac{\partial}{\partial y} \left(\frac{\partial u_\delta}{\partial x} \right) \right] - \frac{F^2}{2} + \frac{\partial}{\partial \hat{\eta}} \left(\mathcal{K}^2 l_0 \frac{\partial F}{\partial \hat{\eta}} \right) \tag{4}$$

Energy:

$$\tilde{V} \frac{\partial g}{\partial \hat{\eta}} = \frac{\partial}{\partial \hat{\eta}} \left(\mathcal{K}^2 \frac{l_0}{Pr} \frac{\partial g}{\partial \hat{\eta}} \right) - \frac{\partial}{\partial \hat{\eta}} \left(\mathcal{K}^2 \frac{l_0}{Pr} \sum_{i=1}^{N_{\mathrm{sp}}} \frac{\partial y_i}{\partial \hat{\eta}} \frac{h_i}{h_\delta} \right) - \frac{\partial}{\partial \hat{\eta}} \left(\mathcal{K} \sum_{i=1}^{N_{\mathrm{sp}}} \tilde{\mathcal{J}}_i^{\hat{\eta}} \frac{h_i}{h_\delta} \right) \tag{5}$$

The dimensionless diffusion flux $\tilde{\mathcal{J}}_i^{\hat{\eta}}$ is defined as $J_{i.}^{y} / \sqrt{(2\rho_\delta \mu_\delta \partial u_\delta / \partial x)}$ and the dimensionless mass production rate $\dot{\mathcal{W}}_i$ as $(\dot{\omega}_i / \rho) / (2 \partial u_\delta / \partial x)$. The boundary conditions for the transformed variables are as follows. At the wall $F = 0$ and $g = h_w / h_\delta$, whereas at the outer edge $F = 1$ and $g = 1$. On the other hand, the boundary conditions for the physical variable are at the wall $u = 0$, $v = 0$, $h = h[T_w(x)]$, and $J_{w,i}^{y} = \dot{\omega}_{i,\mathrm{cat}}$, whereas at the outer edge $u = u_\delta(x)$, $h = h_\delta(x)$, $y_i = y_{\delta,i}(x)$. To solve for the differential problem introduced earlier, one needs to evaluate the thermodynamic, transport, and chemical properties of the mixture. In the VKI boundary-layer code[4] a detailed computation of thermodynamic properties of monoatomic and polyatomic species is performed by means of statistical thermodynamics.[2] The diffusion fluxes are obtained solving for the Stefan–Maxwell equations.[4,6] The chemical nonequilibrium is described by a set of chemical reactions characterized by reaction rates for which data have been found in the literature.[7,8]

The bulk reactions give a contribution to $\dot{\omega}_i$, which can be expressed as follows. For a set of N_r one-step reactions of the type

$$\sum_{i=1}^{N_{\mathrm{sp}}} \nu_{i,r}^{'} X_i \underset{k_{b,r}}{\overset{k_{f,r}}{\rightleftharpoons}} \sum_{i=1}^{N_{\mathrm{sp}}} \nu_{i,r}^{''} X_i$$

the source term related to mass production reads

$$\dot{\omega}_i = M_i \sum_{r=1}^{N_r} (\nu_{i,r}^{''} - \nu_{i,r}^{'}) k_{f,r} \left\{ \prod_{i=1}^{N_{\mathrm{sp}}} c_i^{\nu_{i,r}^{'}} - \frac{1}{K_{c,r}} \prod_{i=1}^{N_{\mathrm{sp}}} c_i^{\nu_{i,r}^{''}} \right\} \tag{6}$$

where $k_{f,r}$ and $K_{c,r}$ are the forward and the equilibrium reaction-rate constants for the rth reaction.

As far as the gas–solid interaction is concerned, the surface reactions define the boundary conditions for the species continuity equations. Indeed, the amount of species i produced or consumed by the surface reactions has to be balanced by the diffusion flux of species i itself. Therefore the boundary condition is $\boldsymbol{J}_{w,i} \cdot \boldsymbol{n} = \dot{\omega}_{i,\mathrm{cat}}$. The next paragraph will be focused on the modeling of the term $\dot{\omega}_{i,\mathrm{cat}}$.

Catalytic Wall Boundary Condition

The recombination phenomenon happening at the solid surface can be represented by a set of N_r heterogeneous reactions. The

modeling of the way in which the species involved in these reactions exchange atoms aims to express the mass production term $\dot{\omega}_{i,\mathrm{cat}}$ as a function of known quantities. Scott[9] proposes a model of the boundary conditions for the species equations based on the following expression for the net mass flux of species i at the surface

$$\dot{\omega}_{i,\mathrm{cat}} = M_i \mathcal{M}_i^{\downarrow} \sum_{r=1}^{N_r} \nu_{ri} \gamma^r - \sum_{r=1}^{N_r} \sum_{j=1}^{N_{\mathrm{sp}}} \mu_{ijr} \gamma^r M_j \mathcal{M}_j^{\downarrow} \tag{7}$$

The matrix ν_{ri} indicates which ith reactants collide upon the surface in the rth reaction, whereas the matrices μ_{ijr} define the jth incident reactants producing the ith products for the rth reaction. Within the methodology followed for the determination of catalytic properties of TPS materials, the reaction probability γ^r is supposed to be independent from the reaction and equal to an effective recombination probability γ_w.

Therefore, the expression for the impinging flux $\mathcal{M}_i^{\downarrow}$, if the Chapman–Enskog perturbation term is considered, reads

$$\mathcal{M}_i^{\downarrow} = [2/(2-\gamma_w)] n_i \sqrt{kT_w/2\pi M_i}$$

This formulation ensures a zero net total mass flux at the wall but does not satisfy in general the element conservation; indeed, considering a catalytic surface model constituted by the two reactions $O + O \rightarrow O_2$ and $CO + O \rightarrow CO_2$, one notices a coupling between the two chemical processes. This in some way establishes a link between the reaction probabilities of the two reactions, which is not specified in the previous formulation.

Elaborating further on this consideration, an alternative approach is proposed. Let us define a rate of reaction per unit surface and unit time for the wall reaction χ_k, which represents the frequency at which reactions take place on the surface.

With this in mind, a formalism similar to the one used for bulk reactions is followed. The number of moles produced per unit surface and unit time are given by

$$\frac{\dot{\omega}_i}{M_i} = \sum_{r=1}^{N_r} (\nu_{ir}^{''} - \nu_{ir}^{'}) \chi_r \tag{8}$$

where, for $\nu_{ir}^{'} \neq 0$

$$\chi_r = \gamma_i^r (\mathcal{M}_i^{\downarrow} / \nu_{ir}^{'}) \tag{9}$$

The surface reaction rate χ_r is therefore related to the recombination probability of species i involved in the rth reaction γ_i^r by the relation (9). As the reaction rate χ_r has to be independent of the species i, it results that the species reaction probabilities γ_i^r are linked by the constraints $\gamma_i^r \mathcal{M}_i^{\downarrow} / \nu_{ir}^{'} = \text{constant} = \chi_r$, for all species such that $\nu_{ir}^{'} \neq 0$. In this case the flux of particle $\mathcal{M}_i^{\downarrow}$ is given by $\mathcal{M}_i^{\downarrow} = 2/(2-\gamma_i) n_i \sqrt{[kT_w/(2\pi M_i)]}$, while

$$\gamma_i = \sum_{r=1}^{N_r} \gamma_i^r$$

represents the recombination probability of species i. The computation of the boundary condition for the species continuity equations will therefore consist in firstly calculating χ_r and then evaluating the production term by means of Eq. (8). The purpose of this alternative formulation is not to better describe the physical phenomenon of heterogeneous catalycity, which is hidden in the definition of the different recombination probabilities. But at least, it provides a model that is consistent with both the global mass and element conservation at the wall, as will be demonstrated by numerical experiments. The latter property comes directly from the form of Eq. (8), which is similar to the one of Eq. (6). Moreover, the quantity χ_r depends only on the reaction considered and not on the species involved in it, which represents another similitude with the bulk reaction mechanism.

Elements Balance and Demixing

In the following the conservation equation for the elements is derived. Starting from the ith species continuity equation, one has

$$\mathrm{div}\left(\frac{\rho_i}{M_i} \boldsymbol{u} + \frac{\boldsymbol{J}_i}{M_i} \right) = \frac{\dot{\omega}_i}{M_i}$$

After multiplication by the atomicity coefficient λ_{ij} and summation among all of the species, the preceding equation reads

$$\mathrm{div} \left(\underbrace{\sum_{i=1}^{N_{\mathrm{sp}}} \lambda_{ij} c_i}_{\xi_j} \boldsymbol{u} + \sum_{i=1}^{N_{\mathrm{sp}}} \frac{\lambda_{ij} \boldsymbol{J}_i}{M_i} \right) = \sum_{i=1}^{N_{\mathrm{sp}}} \lambda_{ij} \frac{\dot{\omega}_i}{M_i} \tag{10}$$

where $c_i = \rho_i / M_i$ is the number of moles of species i per unit volume and ξ_j, defined as

$$\xi_j = \sum_{i=1}^{N_{\mathrm{sp}}} \lambda_{ij} c_i$$

represents the number of moles of element j per unit volume. Because chemical reactions do not produce or destroy elements, the right term of Eq. (10) is zero. The distribution of elements concentrations ξ_j is thus governed by

$$\mathrm{div}\left(\xi_j \boldsymbol{u} + \sum_{i=1}^{N_{\mathrm{sp}}} \lambda_{ij} \frac{\boldsymbol{J}_i}{M_i} \right) = 0 \tag{11}$$

where $j = 1$ for oxygen and $j = 2$ for carbon.

The element fraction can therefore change along a streamline thanks to diffusion phenomena. It is important to underline that chemistry has no influence in this balance because it represents only a way in which atoms can be exchanged between various species.

Let us now consider the global elemental balance over the control volume consisting of a cylinder of height δ and radius x around the stagnation line (Fig. 1). The elemental balance equation is

$$\underbrace{\xi_{j\delta} V_\delta}_{①} + \underbrace{\sum_{i=1}^{N_{\mathrm{sp}}} \lambda_{ij} \frac{J_{\delta,i}^y}{M_i}}_{②} - \underbrace{\sum_{i=1}^{N_{\mathrm{sp}}} \lambda_{ij} \frac{J_{w,i}^y}{M_i}}_{③} + \underbrace{2 \frac{\partial u_\delta}{\partial x} \frac{\delta}{\int_0^{\hat{\eta}_{\max}} (d\hat{\eta}/\rho)} \int_0^{\hat{\eta}_{\max}} \xi_j \frac{F(\hat{\eta})}{\rho} d\hat{\eta}}_{④} = 0 \tag{12}$$

where ① and ④ are the elemental convection fluxes through the top surface (boundary-layer edge) and through the lateral surface, respectively, and ② and ③ are the elemental diffusion fluxes through the top (boundary-layer edge) and bottom (solid wall) surfaces.

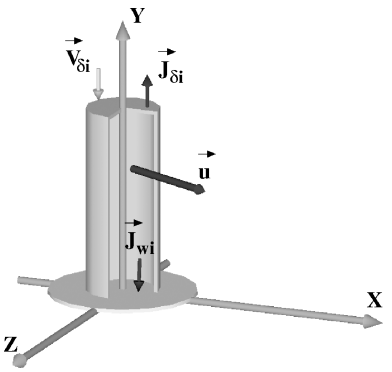

Fig. 1 Control volume for the determination of the global elemental balance Eq. (12).

Now, assuming a nonablating wall, elements are neither created or destroyed at the wall and therefore the elemental diffusion flux at the wall ③ must be identically zero. As the elemental diffusion flux through the boundary layer edge ② is generally negligible, the sum of convective fluxes ① and ④ must vanish. This conclusion will be used for the analysis of the computational results.

Thermodynamic Analysis

In this section thermodynamic properties of dissociating and ionizing CO_2 mixtures are analyzed in order to identify suitable mixture definitions over certain temperature ranges. Pure CO_2 is considered because the experiments needed to estimate catalytic properties of TPS materials will first be carried out in VKI facilities using pure CO_2, which is the major component of Mars atmosphere.[10]

The first step in the determination of the species required for the simulation of a multispecies flow consists in defining a reference mixture. In the present case it consists of the following 11 species: CO_2, O_2, CO, C, O, CO_2^+, O_2^+, CO^+, C^+, O^+, and e^-.

The equilibrium composition of such a mixture as a function of temperature is shown in Fig. 2, and in terms of mole fraction in Fig. 3, starting from pure CO_2 at $T = 300$ K. The evolution of mole fractions shows the existence of a threshold above which is necessary to take ionization into account and below which the ionized species can be neglected. The choice of this temperature equal to $T^* = 7000$ K leads to the definition of two different mixtures. Figure 4 shows the specific heat at constant pressure as a function of temperature for different mixtures used, in order to determine the minimum number of species required to describe, within a certain accuracy, the energetic behavior of the reference mixture.

The $C_p(T)$ of the reference mixture is characterized by the presence of three peaks around 3000, 7000, and 12,000 K, respectively, which actually correspond to the dissociation of CO_2, O_2, and CO and ionization of carbon and atomic oxygen.

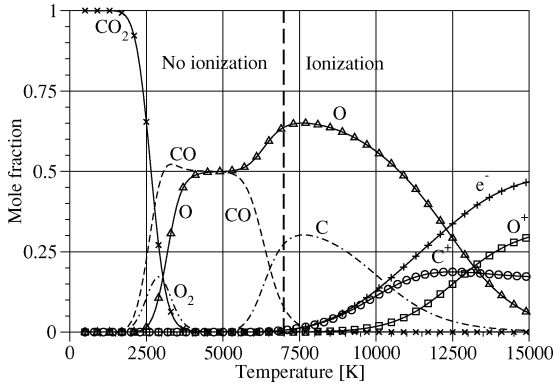

Fig. 2 Equilibrium composition of the reference mixture for pure CO_2 flows at 0.1 atm.

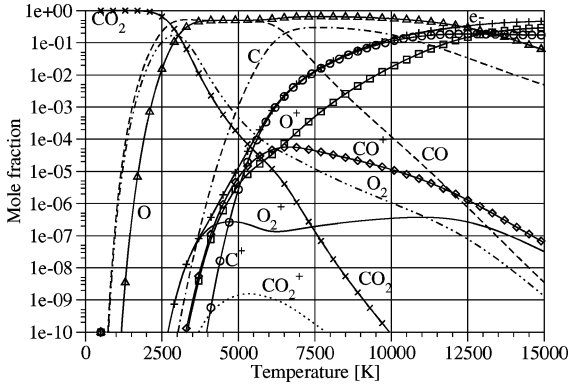

Fig. 3 Logarithm of equilibrium mole fractions for the lower components of the reference mixture for pure CO_2 flows at 0.1 atm.

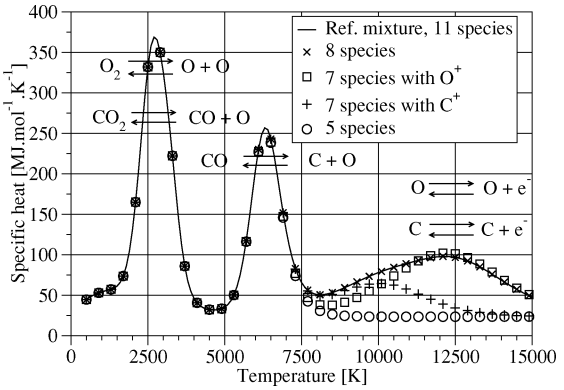

Fig. 4 Equilibrium C_p of various candidate mixtures at 0.1 atm.

Below the threshold temperature, the five-species mixture is characterized by a C_p that is close enough to the one of the reference mixture one aims to simulate. Above this temperature it is necessary to account for ionized species, and there is a possibility of augmenting the preceding mixture choosing among CO_2^+, CO^+, O_2^+, O^+, C^+, and of course e^-.

From the analysis of Fig. 3, it turns out that the presence of both O^+ and C^+ must be taken into account.

To verify the quality of the preceding choices, the relative errors committed in the calculation of the C_p for different mixtures have been computed. In particular, for temperatures lower than T^* the relative error computed as

$$\Delta Cp_{\text{rel}} = \frac{|Cp_{\text{mixture}} - Cp_{\text{ref}}|}{Cp_{\text{ref}}} 100 \tag{13}$$

is less than 5% for all of the considered mixtures, whereas above this temperature it is only so for the eight-species mixture already introduced, which shows the quality of the selected models.

Stagnation-Line Flow Computations

In this section are presented the results obtained for several cases defined by Kolesnikov and colleagues in Refs. 11 and 12 referring to the 100-kW IPG-4 plasmatron (IPM). Many calculations have been carried out at VKI[13] covering a wide range of enthalpy conditions. In this paper two cases corresponding to extreme enthalpy values will be considered: 1) low-enthalpy case, where mixture enthalpy at the outer edge $h_e = 15.3$ MJ/kg, incoming flow velocity $V_s = 115$ m/s, and pressure $p = 5.8 \cdot 10^{-2}$ atm; and 2) high-enthalpy case, where $h_e = 39$ MJ/kg, $V_s = 164$ m/s, and $p = 0.1$ atm. The flow is taken to be in LTE conditions at the boundary-layer edge. Therefore, the outer edge temperature is the result of an iterative calculation in which the thermodynamic modeling of the flow plays an important role. The corresponding values of temperature are 5922 and 8127 K for the low- and high-enthalpy cases, respectively.

For the given flow conditions at the boundary-layer edge, the heat flux at the stagnation point of the model has been computed as a function of the surface temperature T_w and the surface effective catalycity γ_w from the solution of the stagnation line equations. The analysis of the nonequilibrium dissociated subsonic flow around the model is based on the assumptions discussed at the beginning of this paper and on the following ones:

1) The gas is represented by a five-species (CO_2, CO, O_2, O, C) viscous and heat-conductive mixture.

2) The reaction set describing the finite-rate bulk chemistry of the flow is the one described here:

The dissociation reactions are

$$CO_2 + M \rightleftarrows CO + O + M$$

$$CO + M \rightleftarrows C + O + M$$

$$O_2 + M \rightleftarrows O + O + M$$

and the neutral exchange reactions are

$$CO + O \rightleftarrows C + O_2$$

$$CO_2 + O \rightleftarrows CO + O_2$$

3) The surface catalytic reactions proceed according to the Eley–Rideal mechanism, and the following models are considered for the various cases analyzed:

a)

$$O + (O - S) \rightarrow O_2 + S$$

$$CO + (O - S) \rightarrow CO_2 + S$$

b)

$$O + (O - S) \rightarrow O_2 + S$$

$$CO + (O - S) \rightarrow CO_2 + S$$

$$C + 2(O - S) \rightarrow CO_2 + 2S$$

Another important assumption in the present model is that all of the recombining species have the same effective recombination probability, that is, for the mentioned wall chemistry model one has $\gamma_{CO_w} = \gamma_{O_w} = \gamma_{C_w} = \gamma_w$.

As the result of the computations performed along the stagnation line, for a 50-mm-diam probe several charts have been determined for the stagnation point heat flux as a function of T_w and $\gamma_w \in [0, 1]$ and will be presented later in this section.

Low-Enthalpy Case

The low-enthalpy case is considered first. For this case only the two-surface reactions model has been applied, using both Scott's model and the present formulation. For this two-surface reactions model the present formulation reads

$$\gamma_O^1 + \gamma_O^2 = \gamma_O = \gamma_w, \qquad \gamma_{CO}^2 = \gamma_{CO} = \gamma_w$$

$$\gamma_O^2 \mathcal{M}_O^{\downarrow} = \gamma_{CO}^2 \mathcal{M}_{CO}^{\downarrow}$$

This constitutes a 3×3 system in the unknowns $\gamma_O^1, \gamma_O^2, \gamma_{CO}^2$, which must also satisfy the inequalities $0 \le \gamma_i^r \le \gamma_w$. The solution is easily obtained:

$$\gamma_{CO}^2 = \gamma_w, \qquad \gamma_O^2 = \gamma_{CO}^2 \frac{\mathcal{M}_{CO}^{\downarrow}}{\mathcal{M}_O^{\downarrow}}, \qquad \gamma_O^1 = \gamma_w - \gamma_O^2$$

This solution is valid as long as $\gamma_O^2 \le \gamma_w$. If it is not, then it means that one of the assumptions made does not hold (e.g., equal recombination probability for all species). In practice, γ_O^2 was always below γ_w for our computations. Then, the reaction frequencies are obtained as

$$\chi_1 = \frac{\gamma_O^1 \mathcal{M}_O^{\downarrow}}{2} \qquad \text{and} \qquad \chi_2 = \gamma_{CO}^2 \mathcal{M}_{CO}^{\downarrow}$$

leading to the following expressions for the species production terms:

$$\frac{\dot{\omega}_{CO_2}}{M_{CO_2}} = \gamma_{CO}^2 \mathcal{M}_{CO}^{\downarrow}, \qquad \frac{\dot{\omega}_C}{M_C} = 0, \qquad \frac{\dot{\omega}_{O_2}}{M_{O_2}} = \frac{\gamma_O^1 \mathcal{M}_O^{\downarrow}}{2}$$

$$\frac{\dot{\omega}_O}{M_O} = -\left(\gamma_O^1 + \gamma_O^2\right) \mathcal{M}_O^{\downarrow}, \qquad \text{and} \qquad \frac{\dot{\omega}_{CO}}{M_{CO}} = -\gamma_{CO}^2 \mathcal{M}_{CO}^{\downarrow}$$

All of the computations shown in the following are converged for a 100-points discretization of the stagnation line. A grid resolution was conducted to obtain reliable heating predictions. Species mass fraction and nondimensional temperature profiles along the stagnation line are shown in Fig. 5 for 100- and 200-point grids, for both the McKenzie (Fig. 5a) and Park (Fig. 5b) bulk chemistry models.

Table 1 Wall heat flux for several boundary conditions (Park chemistry model) (h_e = 15.3 MJ/kg, T_w = 300 K)

Boundary condition	q_w, MW/m^2
FCW	0.856
LEW—$x_{n,\mathrm{FC}}$	0.857
LEW—$x_{n,\delta}$	0.918

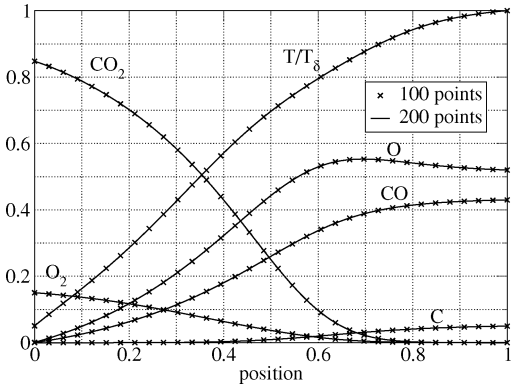

a) McKenzie bulk chemistry model

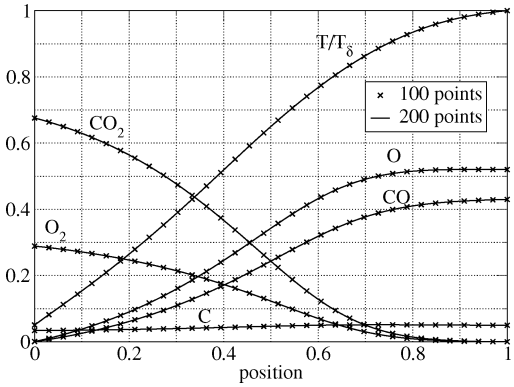

b) Park bulk chemistry model

Fig. 5 Grid-convergence analysis (present wall chemistry model): h_e = 15.3 MJ/kg and T_w = 300 K; 0, wall; 1, δ.

The solutions for both mesh refinements are seen to be identical, showing the grid independence of the results.

The diffusion demixing phenomenon is analyzed by considering three different boundary conditions: fully catalytic wall (present wall chemistry model—FCW); equilibrium wall with the element fraction of the outer edge (LEW—$x_{n,\delta}$); equilibrium wall with the element fraction corresponding to the fully catalytic case (LEW—$x_{n,\mathrm{FC}}$). The wall heat flux corresponding to these cases is summarized in Table 1.

Assuming a local equilibrium with the outer edge elemental fraction results in an overestimation of the wall heat flux, which is explained as follows. The wall heat flux is primarily controlled by the recombination processes taking place at the wall. Because of diffusion demixing in the boundary layer, there is more oxygen and less carbon at the wall then at the outer edge (see Fig. 6, which shows the mass fraction profiles for the three boundary conditions). As a result, fewer CO_2 molecules can be formed, the excess oxygen forming O_2 molecules. Hence, less heat is released than if C and O elements were in the $\frac{1}{3}$–$\frac{2}{3}$ proportion.

These results point out the importance of diffusion demixing effects, in particular regarding their influence on wall heat flux, and clearly establishes that the local equilibrium boundary condition based on outer edge (freestream) elemental fractions is incorrect.[14,15]

Another illustration of the importance of this phenomenon is provided by comparing Scott's and the present formulation for a fully

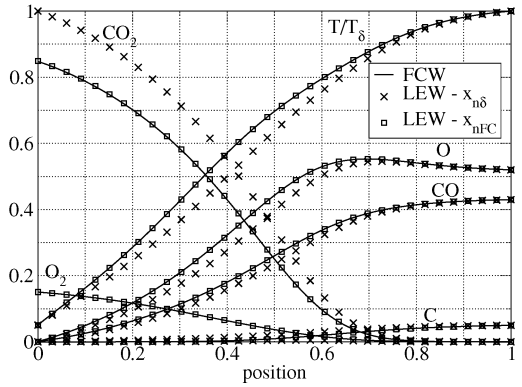

Fig. 6 Mass fractions and nondimensional temperature for three different boundary conditions (Park bulk chemistry model): h_e = 15.3 MJ/kg, and T_w = 300 K.

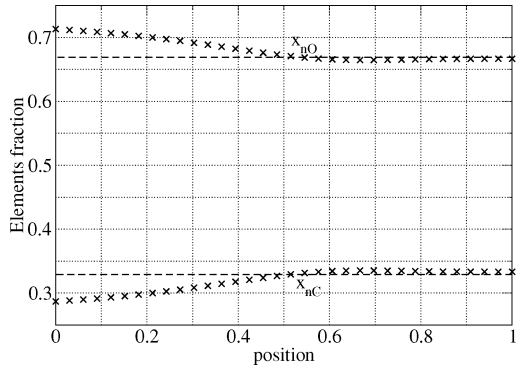

a) Scott wall chemistry model

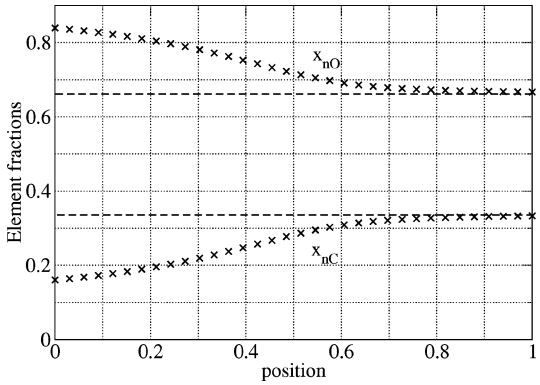

b) Present wall chemistry model

Fig. 7 Element fractions computed with the Scott's and the present catalycity models (Park bulk chemistry model): 0, wall; 1, δ.

catalytic wall. Computed elemental fraction profiles are presented in Fig. 7, always for the low-enthalpy case. Elemental fractions of carbon ($x_{n\mathrm{C}}$) and oxygen ($x_{n\mathrm{O}}$) are defined as

$$x_{n\mathrm{O}} = \frac{\xi_{\mathrm{O}}}{\xi_{\mathrm{C}} + \xi_{\mathrm{O}}} \qquad \text{and} \qquad x_{n\mathrm{C}} = \frac{\xi_{\mathrm{C}}}{\xi_{\mathrm{C}} + \xi_{\mathrm{O}}}$$

where

$$\xi_{\mathrm{C}} = (x_{\mathrm{CO_2}} + x_{\mathrm{CO}} + x_{\mathrm{C}})\frac{p}{\mathcal{R}T}$$

and

$$\xi_{\mathrm{O}} = \left(2x_{\mathrm{CO_2}} + x_{\mathrm{CO}} + 2x_{\mathrm{O_2}} + x_{\mathrm{O}}\right)\frac{p}{\mathcal{R}T}$$

with $\mathcal{R}$ being the universal gas constant. One observes that for Scott's formulation, $x_{n\mathrm{O}} > x_{n\mathrm{O},\delta}$ throughout the boundary layer, which is in contradiction with the elemental balance [Eq. (12)]. Indeed, as discussed earlier, only convective fluxes are significant in the elemental balance (the wall diffusion flux is zero and the edge diffusion flux is negligible) so that Eq. (12) reduces to

$$\xi_{j\delta} V_\delta + 2\frac{\partial u_\delta}{\partial x}\left(\delta \Big/ \int_0^{\hat{\eta}_{\max}} \frac{\mathrm{d}\hat{\eta}}{\rho}\right)\int_0^{\eta_{\max}} \xi_j \frac{F(\hat{\eta})}{\rho}\,\mathrm{d}\hat{\eta} = 0 \qquad (14)$$

Hence, the elemental concentration ξ_j distribution must be such that some weighted average of it equals the outer edge concentration and similarly for the elemental fraction x_{nj}, which is not verified when $x_{n\mathrm{O}} > x_{n\mathrm{O},\delta}$ throughout the boundary layer. In contrast, the elemental fraction distributions obtained with the present wall chemistry model are compatible with this condition (Fig. 7b).

In fact, the elemental fraction distribution obtained with Scott's wall chemistry model violates this condition because this model does not respect elemental conservation at the wall. For the present problem it provides a source of O and a sink of C at the wall. This was verified by computing the elemental diffusion fluxes at the wall and observing that

C:

$$\frac{J^y_{\mathrm{CO_2}w}}{M_{\mathrm{CO_2}}} + \frac{J^y_{\mathrm{CO}w}}{M_{\mathrm{CO}}} + \frac{J^y_{\mathrm{C}w}}{M_{\mathrm{C}}} < 0$$

O:

$$2\frac{J^y_{\mathrm{CO_2}w}}{M_{\mathrm{CO_2}}} + \frac{J^y_{\mathrm{CO}w}}{M_{\mathrm{CO}}} + 2\frac{J^y_{\mathrm{O_2}w}}{M_{\mathrm{O_2}}} + \frac{J^y_{\mathrm{O}w}}{M_{\mathrm{O}}} > 0$$

We now analyze the calculated heat-flux maps for the present flow conditions. Heat-flux maps consist of curves of wall heat flux q_w as a function of wall temperature between 300 and 2100 K for various values of the recombination probability γ_w. Four different maps have been obtained for the present test case, corresponding to all possible bulk chemistry (Park/McKenzie) and wall chemistry (Scott/present) model combinations. They are displayed in Fig. 8.

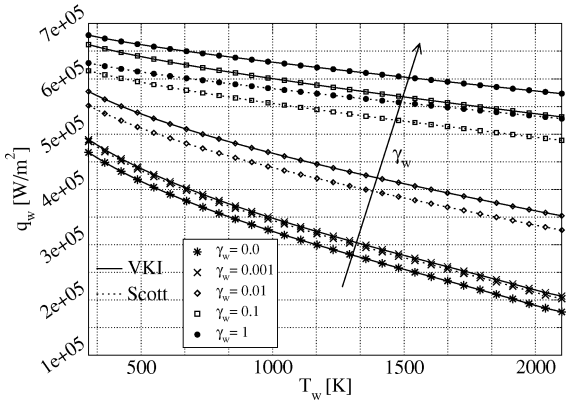

a) McKenzie bulk chemistry model

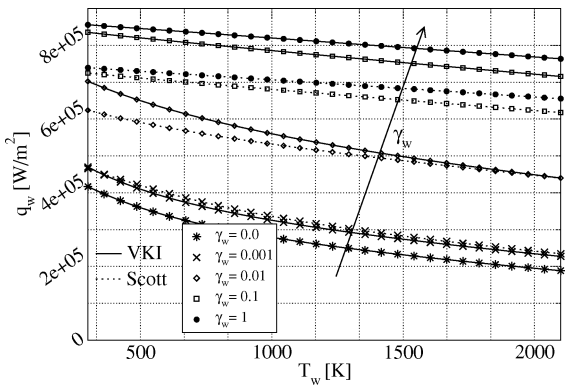

b) Park bulk chemistry model

Fig. 8 Heat-flux maps for the lower-enthalpy case: h_e = 15.3 MJ/kg.

The influence of the bulk chemistry model is clearly visible. Park's model reaction rates being much larger than McKenzie's, the wall heat flux is significantly larger for low wall temperatures and low recombination probabilities. The influence of the wall reaction model is also important for large recombination probabilities. For high values of catalycity, the heat flux is seen to be significantly higher with the present model, which is consistent with the fact that, because of the existence of a sink of C atoms at the wall in Scott's model, there are fewer C atoms available for recombination.

High-Enthalpy Case

Attention is now turned to the high-enthalpy case. Because of the higher enthalpy level, the mass fraction of C atom at the outer edge is much higher, so that the third wall reaction $C + 2(O - S) \rightarrow CO_2$ can become important. For this reason we first analyze the influence of the wall reactions set using Scott's formulation for both bulk chemistry models. Species mass fractions and nondimensional temperature profiles are shown in Fig. 9 for a fully catalytic wall. Whereas for Park's model there is no influence of the wall reactions set because the carbon atom entirely recombines inside the boundary layer (bulk chemistry), on the contrary the wall reactions set has a large influence when using McKenzie's model, for which bulk reactions are much slower.

In particular, if the third wall reaction is ignored there remains an important amount of atomic carbon at the wall. As a result, the wall heat flux is considerably smaller (see Table 2 in which heat fluxes are listed for all bulk chemistry/wall reaction set combinations).

The present formulation for the three-wall-reaction model reads as follows:

$$\gamma_O^1 + \gamma_O^2 + \gamma_O^3 = \gamma_O = \gamma_w, \qquad \gamma_{CO}^2 = \gamma_{CO} = \gamma_w$$

$$\gamma_C^3 = \gamma_C = \gamma_w, \qquad \gamma_O^2 \mathcal{M}_O^{\downarrow} = \gamma_{CO}^2 \mathcal{M}_{CO}^{\downarrow}, \qquad \gamma_C^3 \mathcal{M}_C^{\downarrow} = \frac{\gamma_O^3 \mathcal{M}_O^{\downarrow}}{2}$$

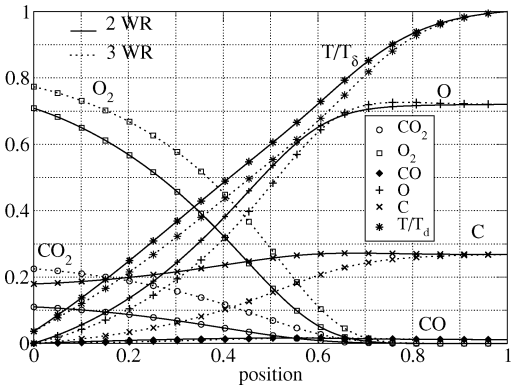

a) McKenzie bulk chemistry model

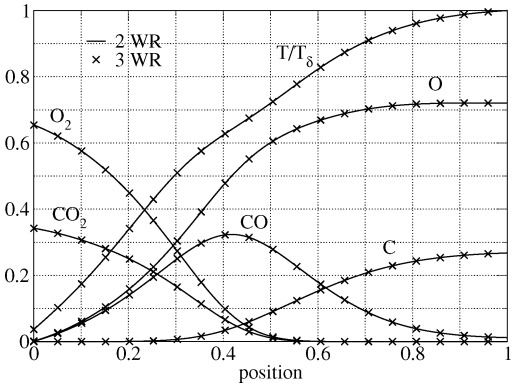

b) Park bulk chemistry model

Fig. 9 Mass fractions and nondimensional temperature profile: h_e = 39 MJ/kg, T_w = 300 K, 0, wall; 1, δ.

Table 2 Wall heat flux for several sets of surface reactions (h_e = 39 MJ/kg, T_w = 300 K)

Surface	Stagnation line	q_w, MW/m^2
Scott 2WR	McKenzie	1.20
Scott 3WR	McKenzie	2.14
Scott 3WR	Park	2.23
Scott 2WR	Park	2.24

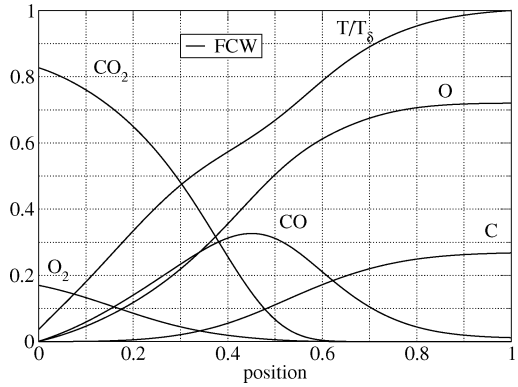

Fig. 10 Mass fractions and nondimensional temperature profile (Park bulk chemistry model): h_e = 39 MJ/kg, T_w = 300 K; 0, wall; 1, δ.

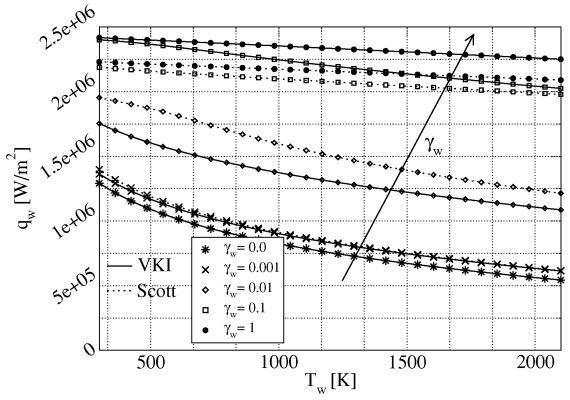

Fig. 11 Heat-flux map for the higher enthalpy (Park bulk chemistry model): h_e = 39 MJ/kg.

i.e., a system of five equations in five unknowns γ_O^1, γ_O^2, γ_O^3, γ_{CO}^2, and γ_C^3. For the present flow conditions numerical experiments have shown that the solution does not satisfy the constraint $\gamma_O^3 \leq \gamma_w$, which implies that the hypothesis of equal recombination probabilities for all species does not hold. The analysis of a suitable assumption is however out of the scope of the present paper.

It was therefore decided to switch our attention to the Park bulk chemistry/two-wall-reaction model for the present high-enthalpy case.

Species mass fraction and nondimensional temperature profiles for a fully catalytic wall computed using the present wall chemistry formulation are shown in Fig. 10. This is to be compared with Fig. 9b, where Scott's formulation was used. The same conclusion as for the low-enthalpy case is obtained, that is, for high γ_w Scott's model acts as a sink of carbon atoms at the wall. As a result, the wall heat flux is smaller, as seen in Fig. 11, which shows the heat-flux map for the high-enthalpy case.

Conclusions

A numerical study of the nonequilibrium stagnation-line flow of a carbon dioxide mixture has been presented.

For temperatures below 7000 K, typical of entry applications, a five-species model has been shown to be suitable, whereas an eight-species model is required for higher temperatures, for LTE inductively coupled plasma flow computations, for instance. It was

shown that the wall chemistry model of Scott does not satisfy elemental conservation at the wall. To remedy this problem, an alternative model was proposed and tested. Numerical results show a significant influence of the wall chemistry model: wall heat fluxes obtained using the present formulation are substantially higher than those obtained using Scott's model for high values of catalycity because the latter model acts as a sink of carbon atoms at the wall.

Numerical results also show the importance of diffusion demixing, as illustrated by the significant variation of elemental fractions across the boundary layer.

References

[1]Kolesnikov, A. F., "Extrapolation from High Enthalpy Tests to Flight Based on the Concept of Local Heat Transfer Simulation," *Measurements Techniques for High Enthalpy and Plasma Flows*, edited by J. M. Charbonnier and G. S. R. Sarma, NATO-RTO von Kármán Inst., Rhode-St-Genése, Belgium, 1999, Chap. 8A.

[2]Bottin, B., Vanden Abeele, D., Carbonaro, M., Degrez, G., and Sarma, G. S. R., "Thermodynamic and Transport Properties for Inductive Plasma Modeling," *Journal of Thermophysics and Heat Transfer*, Vol. 13, No. 3, 1999, pp. 343–350.

[3]Magin, T., Degrez, G., and Sokolova, I., "Thermodynamic and Transport Properties of Martian Atmosphere for Space Entry Application," AIAA Paper 02-2226, May 2002.

[4]Barbante, P. F., Degrez, G., and Sarma, G. S. R., "Computation of Nonequilibrium High-Temperature Axisymmetric Boundary-Layer Flows," *Journal of Thermophysics and Heat Transfer*, Vol. 16, No. 4, 2002, pp. 490–497.

[5]Degrez, G., Barbante, P., de la Llave, M., Magin, T., and Chazot, O., "Determination of the Catalytic Properties of TPS Materials in the VKI ICP Facilities," ECCOMAS Computational Fluid Dynamics Conference 2001 [CD-ROM], European Community on Computational Methods in Applied Sciences, Regensburg, Germany, Sept. 2001.

[6]Kolesnikov, A. F., "Self-Consistent Stefan–Maxwell Relations for Multi-Component Ambipolar Diffusion in Two-Temperture Plasma Mixtures," von Karman Inst. for Fluid Dynamics, Tech. Rept. VKI TN-196, Rhode-Saint-Genèse, Belgium, Jan. 1999.

[7]Park, C., Howe, J. T., and Jaffe, R. L., "Review of Chemical-Kinetic Problems of Future NASA Mission, II: Mars Entries," *Journal of Thermophysics and Heat Transfer*, Vol. 8, No. 1, 1994, pp. 9–23.

[8]McKenzie, R. L., "An Estimate of the Chemical Kinetics Behind Normal Shock Waves in Mixtures of Carbon Dioxide," NASA TN D-3287, Feb. 1966.

[9]Scott, D. C., "Catalytic Boundary Conditions in Nonequilibrium Flow," *Proceeding of IUTAM Symposium Marseille*, edited by R. Brun and A. A. Chikhaoui, Dept. Milleux Hors d'Equilibre, Université de Provence, Marseille, France, 1992, pp. 298–305.

[10]Seiff, A., and Kirk, D. B., "Structure of the Mars Atmosphere in Summer at Mid-Latitudes," *Geophysical Research*, Vol. 82, No. 28, 1977, pp. 4364–4378.

[11]Kolesnikov, A. F., Pershin, I. S., Vasil'evskii, S. A., and Yakushin, M. I., "Study of Quartz-Surface Catalycity in Dissociated Carbon Dioxide Subsonic Flows," *Journal of Spacecraft and Rockets*, Vol. 37, No. 5, 2000, pp. 573–579.

[12]Kolesnikov, A. F., and Marraffa, L., "An Analysis of Stagnation Point Thermochemical Simulation by Plasmatron for Mars Probe," AIAA Paper 99-3564, June–July 1999.

[13]Rini, P., "Numerical Simulation of Equilibrium and Non Equilibrium CO_2 Plasma Flows," von Karman Inst. for Fluid Dynamics, Tech. Rept. VKI PR 2002-22, Rhode-Saint-Genèse, Belgium, June 2002.

[14]Rini, P., Nannipieri, N., Chazot, O., and Degrez, G., "Numerical Simulation of Thermochemical Equilibrium Boundary Layers," Paper NCTAM-2003-019, 6th National Congress Theoretical and Applied Mechanics, University of Gent, Gent, Belgium, May 2003.

[15]Rini, P., Magin, T., Degrez, G., Fletcher, D., "Numerical Simulation of Non Equilibrium Hypersonic CO_2 Flows for Mars Entry Application," Paper 24_094_P, 3rd International Symposium Atmospheric Reentry Vehicles and Systems, Association Aéronautique et Astronautique de France, Verneuil-sur-Seine, France, March 2003.